ELSEVIER

Chemical Engineering Journal 97 (2004) 37–45

Chemical Engineering Journal

www.elsevier.com/locate/cej

Analytic solution of the Maxwell–Stefan equations for multicomponent permeation across a zeolite membrane

R. Krishna*, R. Baur

Department of Chemical Engineering, University of Amsterdam, Nieuwe Achtergracht 166, 1018 WV Amsterdam, The Netherlands

Received 31 January 2003; accepted 1 June 2003

Abstract

We develop an analytic solution of the Maxwell–Stefan equations describing steady-state diffusion of *n*-component mixtures across a zeolite membrane. In the development of the analytic solution we assume Langmuirian behaviour of the pure components and that the mixture sorption can be calculated from the multicomponent Langmuir isotherm. Explicit expressions are derived for calculation of steady-state fluxes and the loading profiles in the membrane. The utility of the developed solution is illustrated by means of two illustrative examples involving permeation of alkane mixtures across an MFI membrane.

Keywords: Maxwell–Stefan theory; Zeolite membrane permeation; Separation of alkanes

1. Introduction

There is increasing interest in the use of zeolite membranes for separation of mixtures relying on differences in the permeation fluxes [1–3]. Zeolite membranes are also used for in situ separation within a reactor [4]. The permeation flux of a component is determined by the adsorption and diffusion characteristics of all the components in the mixture, and separation selectivities cannot be estimated from single component permeation data alone [5]. The proper description of zeolite membrane permeation must take account of the subtle interplay between adsorption and diffusion, and also the coupling between species diffusion [5]. Due to coupling in the species diffusion, the faster moving species are slowed down and, concomitantly, the more sluggish species are accelerated [6,7].

It is now widely accepted that for proper description of multicomponent diffusion across zeolite membranes, we must use the Maxwell–Stefan (M–S) formulation [5,8–12]. Indeed, many recent studies have made use of the M–S equations to interpret measured experimental data on permeation [13–16]. For *single* component permeation the M–S equations can be solved analytically, for the case in which the boundary conditions on either side of the membrane are fixed [17]. For two-component permeation, Kerkhof [18] has presented a *partial* analytic solution. The major objective of the present communication is to develop an *explicit analytic* expression for calculation of the steady-state fluxes for *n*-component permeation across a zeolite membrane. We demonstrate the utility of the developed expression by considering two illustrative examples for separation of mixtures of alkanes using an MFI membrane. The analytic expression is compared with precise numerical solutions following the procedure discussed elsewhere [3,10–12].

2. Model development

In the M–S formulation the chemical potential gradients are written as linear functions of the fluxes [6–9,19–21]:

$$-\rho\frac{\theta_i}{RT}\frac{\partial\mu_i}{\partial z} = \sum_{\substack{j=1\\ j\neq i}}^{n}\frac{q_j N_i - q_i N_j}{q_{i,\mathrm{sat}} q_{j,\mathrm{sat}} \mathcal{D}_{ij}} + \frac{N_i}{q_{i,\mathrm{sat}}\mathcal{D}_i}, \quad i = 1, 2, \ldots, n \tag{1}$$

The fractional occupancies are defined by

$$\theta_i = \frac{q_i}{q_{i,\mathrm{sat}}} \tag{2}$$

where q_i is the molar loading of species i and $q_{i,\mathrm{sat}}$ the saturation loading.

We have to reckon in general with two types of Maxwell–Stefan diffusivities: $\mathcal{D}_i$ and $\mathcal{D}_{ij}$. The $\mathcal{D}_i$ are the diffusivities that reflect interactions between species i and the zeolite

* Corresponding author. Tel.: +31-20-5257007; fax: +31-20-5255604.
E-mail address: krishna@science.uva.nl (R. Krishna).

1385-8947/$ – see front matter © 2003 Elsevier B.V. All rights reserved.
doi:10.1016/S1385-8947(03)00149-9

Nomenclature

b_i	parameter in the pure component Langmuir adsorption isotherm (Pa^{-1})
$[B]$	square matrix of inverse Maxwell–Stefan coefficients (m^{-2} s)
$[B(0)]$	$[B]$ matrix at zero loading (m^{-2} s)
$Đ_i$	Maxwell–Stefan diffusivity of species i (m^2/s)
$Đ_{ij}$	Maxwell–Stefan diffusivity describing interchange between i and j (m^2/s)
$Đ_i(0)$	Maxwell–Stefan diffusivity of species i at zero loading (m^2/s)
N_i	molar flux of species i (mol m^{-2} s^{-1})
p_i	partial pressure of species i (Pa)
q_i	molar loading of component i (mol kg^{-1})
$q_{i,\mathrm{sat}}$	saturation loading of component i (mol kg^{-1})
R	gas constant (8.314 J mol^{-1} K^{-1})
t	time (s)
T	absolute temperature (K)
z	distance coordinate along membrane (m)

Greek letters

$[\Gamma]$	matrix of thermodynamic factors (–)
Γ_{ij}	element of $[\Gamma]$ (–)
δ	thickness of membrane (m)
δ_{ij}	Kronecker delta (–)
η	dimensionless distance (–)
θ_i	fractional occupancy of component i (–)
θ_V	fractional vacancy (–)
μ_i	molar chemical potential (J mol^{-1})
π_i	dimensionless partial pressures, $b_i p_i$ (–)
ρ	density of the membrane (kg m^{-3})

Subscripts

i, j	components in mixture
sat	referring to saturation conditions
V	vacancy
0	upstream face of membrane
δ	downstream face of membrane
η	position along membrane

Vector and matrix notation

$(\cdot)$	component vector
$[\cdot]$	square matrix

matrix; they are also referred to as jump or "corrected" diffusivities in the zeolite literature [11,22,23]. Experimental and molecular dynamics (MD) simulation data for weakly confined guest molecules in zeolitic hosts (e.g. methane, He, Ne, Ar in MFI) show that $Đ_i$ are practically independent of the loading, i.e. occupancy [11,24–27]:

$$Đ_i = Đ_i(0) \tag{3}$$

For diffusion of larger guest molecules, such as CF_4, SF_6 and 2-methylhexane (2-MH) in MFI a different loading dependence of $Đ_i$ has been observed in MD [27] and kinetic Monte Carlo (KMC) simulations [28–30]. These studies show that $Đ_i$ decreases strongly with the loading and follows the relation:

$$Đ_i = Đ_i(0)(1 - \theta_1 - \theta_2 - \cdots - \theta_n) = Đ_i(0)\theta_\mathrm{V} \tag{4}$$

where θ_V is the vacancy:

$$\theta_\mathrm{V} = (1 - \theta_1 - \theta_2 - \cdots - \theta_n) \tag{5}$$

Whether a molecule follows scenario (3) or (4) depends on the degree of confinement within the zeolite host, and on adsorbate–adsorbate interactions [27,31,32].

Fig. 1 portrays the molecular jump processes in: (a) intersecting channel structures, (b) cage-type structures, separated by windows and (c) single-file diffusion in one-dimensional channels. Site-to-site jump leaves behind a vacancy. Subsequent jumps are more likely to fill this vacancy, thus producing "vacancy correlation" effects [7,31]. When the jump of species i creates a vacancy and this vacancy is filled by species j, the vacancy correlation effect is captured by the term containing the "exchange" coefficients $Đ_{ij}$ in Eq. (1). The Onsager reciprocal relations demand $Đ_{ij} = Đ_{ji}$. The net effect of this exchange is a slowing down of a faster moving species due to interactions with a species of lower mobility. Also, a species of lower mobility is accelerated by interactions with another species of higher mobility.

For estimation of the $Đ_{ij}$, Krishna and Wesselingh [8] suggested the logarithmic interpolation formula

$$Đ_{ij} = [Đ_i]^{\theta_i/(\theta_i+\theta_j)}[Đ_j]^{\theta_j/(\theta_i+\theta_j)} \tag{6}$$

For the weak confinement scenario the exchange coefficient is

$$Đ_{ij} = [Đ_i(0)]^{\theta_i/(\theta_i+\theta_j)}[Đ_j(0)]^{\theta_j/(\theta_i+\theta_j)} \tag{7}$$

and for strong confinement the exchange coefficient is given by

$$Đ_{ij} = [Đ_i(0)]^{\theta_i/(\theta_i+\theta_j)}[Đ_j(0)]^{\theta_j/(\theta_i+\theta_j)}\theta_\mathrm{V} \tag{8}$$

The interpolation strategy (6) has been verified by comparison with Monte Carlo and MD simulations [6,7].

For zeolite topologies with high connectivities, the exchange coefficient $Đ_{ij}$ can be expected to be high. For facile particle–particle exchange, i.e. $Đ_{ij} \to \infty$, vacancy correlation effects tend to get washed out. We see from Eq. (1) that when $Đ_{ij} \to \infty$, the flux relations simplify to give

$$N_i = -\rho q_{i,\mathrm{sat}} Đ_i \frac{\theta_i}{RT}\nabla\mu_i, \quad i = 1, 2, \ldots, n \tag{9}$$

The chemical potential gradients in Eq. (1) may be expressed in terms of the gradients of the occupancies by introduction

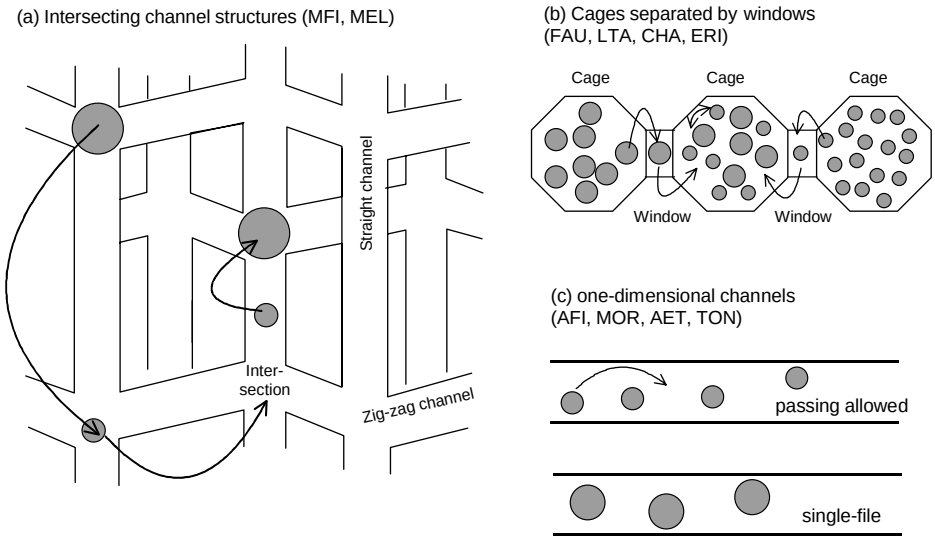

Fig. 1. Pictorial representation of the molecular jumps in: (a) MFI structure, (b) cages separated by windows and (c) single-file diffusion in one-dimensional channels.

of the matrix of thermodynamic factors $[\Gamma]$

$$\frac{\theta_i}{RT}\frac{\partial \mu_i}{\partial z} = \sum_{j=1}^{n} \Gamma_{ij}\frac{\partial \theta_j}{\partial z},$$

$$\Gamma_{ij} \equiv \left(\frac{q_{j,\mathrm{sat}}}{q_{i,\mathrm{sat}}}\right)\frac{q_i}{p_i}\frac{\partial p_i}{\partial q_j} \equiv \frac{\theta_i}{p_i}\frac{\partial p_i}{\partial \theta_j},\ i, j = 1, 2, \ldots, n \qquad (10)$$

where p_i is the partial pressure of component i. We assume that the individual component loadings follow the multicomponent Langmuir isotherm

$$\theta_i = \frac{q_i}{q_{i,\mathrm{sat}}} = \frac{b_i p_i}{1 + \sum_{i=1}^{n} b_i p_i} \equiv \frac{\pi_i}{1 + \sum_{i=1}^{n} \pi_i},\quad i = 1, 2, \ldots, n \qquad (11)$$

where we define the dimensionless partial pressures

$$\pi_i \equiv b_i p_i \qquad (12)$$

Carrying out the differentiation in Eq. (10) the elements of $[\Gamma]$ are

$$\Gamma_{ij} = \delta_{ij} + \frac{\theta_i}{\theta_\mathrm{V}},\quad i, j = 1, 2, \ldots, n \qquad (13)$$

where δ_{ij} is the Kronecker delta. The fractional vacancy θ_V is also given by

$$\theta_\mathrm{V} = (1 - \theta_1 - \theta_2 - \cdots - \theta_n) = \frac{1}{1 + \sum_{j=1}^{n} \pi_j} \qquad (14)$$

Eq. (1) may be recast into n-dimensional matrix expressing the fluxes explicitly as

$$(N) = -\rho[q_{\mathrm{sat}}][B]^{-1}[\Gamma]\frac{\partial(\theta)}{\partial z} \qquad (15)$$

In Eq. (15) $[q_{\mathrm{sat}}]$ is a *diagonal* matrix of saturation capacities $q_{i,\mathrm{sat}}$ and we define the n-dimensional square matrix $[B]$ with elements

$$B_{ii} = \frac{1}{\mathcal{D}_i} + \sum_{\substack{j=1\\ j\neq i}}^{n}\frac{\theta_j}{\mathcal{D}_{ij}},\quad i = 1, 2, \ldots, n,$$

$$B_{ij} = -\frac{\theta_i}{\mathcal{D}_{ij}},\quad i, j\,(i \neq j) = 1, 2, \ldots, n \qquad (16)$$

For weak confinement, the matrix $[B] = [B(0)]$, whose elements are calculated from

$$B_{ii}(0) = \frac{1}{\mathcal{D}_i(0)} + \sum_{\substack{j=1\\ j\neq i}}^{n}\frac{\theta_j}{\mathcal{D}_{ij}},\quad i = 1, 2, \ldots, n,$$

$$B_{ij}(0) = -\frac{\theta_i}{\mathcal{D}_{ij}},\quad i, j\,(i \neq j) = 1, 2, \ldots, n \qquad (17)$$

For strong confinement, we have

$$[B] = [B(0)]\frac{1}{\theta_\mathrm{V}} \qquad (18)$$

The exchange coefficients have to be evaluated using Eq. (7).

Consider a zeolite layer of thickness δ, initially unloaded, subjected at time $t = 0$ to the boundary conditions (see also Fig. 2):

- upstream face:

$$z = 0,\quad p_i = p_{i0},\quad q_i = q_{i0},\quad \theta_i = \theta_{i0},\quad \pi_i = \pi_{i0},\quad \theta_\mathrm{V} = \theta_{\mathrm{V}0} \qquad (19)$$

- downstream face:

$$z = \delta,\quad p_i = p_{i\delta},\quad q_i = q_{i\delta},\quad \theta_i = \theta_{i\delta},\quad \pi_i = \pi_{i\delta},\quad \theta_\mathrm{V} = \theta_{\mathrm{V}\delta} \qquad (20)$$

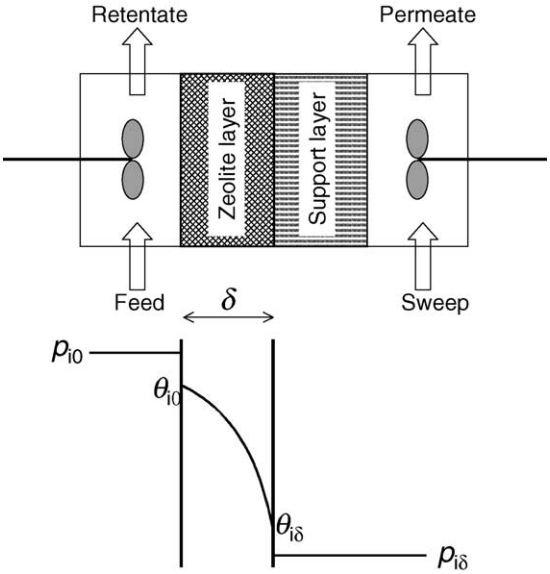

Fig. 2. Schematic representation of zeolite membrane separation device.

The permeation fluxes are obtained by solving

$$\frac{\partial q_i}{\partial t} = -\frac{1}{\rho}\frac{\partial N_i}{\partial z} \tag{21}$$

The steady-state permeation fluxes are given by

$$\frac{\partial (N)}{\partial z} = \frac{\partial}{\partial z}\left(-\rho[q_{\text{sat}}][B]^{-1}[\Gamma]\frac{\partial(\theta)}{\partial z}\right) = (0) \tag{22}$$

Integrating Eq. (22) shows that the N_i are z-invariant, i.e.

$$\begin{aligned}(N) &= -\frac{\rho}{\delta}[q_{\text{sat}}][B_0]^{-1}[\Gamma_0]\left(\frac{\partial(\theta)}{\partial\eta}\right)_{\eta=0}\\ &= -\frac{\rho}{\delta}[q_{\text{sat}}][B_\delta]^{-1}[\Gamma_\delta]\left(\frac{\partial(\theta)}{\partial\eta}\right)_{\eta=1}\end{aligned} \tag{23}$$

where we have defined a dimensionless distance coordinate along the membrane

$$\eta = \frac{z}{\delta} \tag{24}$$

Let us focus on the calculation of $[\Gamma](\partial(\theta)/\partial\eta)$. Using Eqs. (10), (11) and (14) we may write

$$\begin{aligned}\sum_{j=1}^{n}\Gamma_{ij}\frac{\partial\theta_j}{\partial\eta} &= \sum_{j=1}^{n}\frac{\theta_i}{p_i}\frac{\partial p_i}{\partial\theta_j}\frac{\partial\theta_j}{\partial\eta} = \frac{\theta_i}{p_i}\frac{\partial p_i}{\partial\eta}\\ &= \frac{b_i}{\left(1+\sum_{j=1}^{n}\pi_j\right)}\frac{\partial p_i}{\partial\eta} = \frac{1}{\left(1+\sum_{j=1}^{n}\pi_j\right)}\frac{\partial\pi_i}{\partial\eta}\end{aligned} \tag{25}$$

and so we may re-write Eq. (15) in the form

$$\begin{aligned}(N) &= -\frac{\rho}{\delta}[q_{\text{sat}}][B]^{-1}\frac{1}{\left(1+\sum_{j=1}^{n}\pi_j\right)}\frac{\partial(\pi)}{\partial\eta}\\ &= -\frac{\rho}{\delta}[q_{\text{sat}}][B]^{-1}\theta_{\text{V}}\frac{\partial(\pi)}{\partial\eta}\end{aligned} \tag{26}$$

which yields, after re-arrangement

$$\frac{\partial\pi_i}{\partial\eta} = -\left(1+\sum_{j=1}^{n}\pi_j\right)\sum_{j=1}^{n}B_{ij}\frac{N_j\delta}{\rho q_{j,\text{sat}}} = -\frac{1}{\theta_{\text{V}}}\sum_{j=1}^{n}B_{ij}\frac{N_j\delta}{\rho q_{j,\text{sat}}} \tag{27}$$

Summing (27) over the n-species we obtain after introducing Eq. (14)

$$\frac{\partial(1/\theta_{\text{V}})}{\partial\eta} = -\left(\frac{1}{\theta_{\text{V}}}\right)\sum_{i=1}^{n}\sum_{j=1}^{n}B_{ij}\frac{N_j\delta}{\rho q_{j,\text{sat}}} \tag{28}$$

2.1. Analytic solution for weak confinement

For the weak confinement scenario Eq. (3) holds and the summation term on the right-hand side of Eq. (28), after substituting the expressions (17) for $B_{ij} = B_{ij}(0)$ simplifies to give

$$\sum_{i=1}^{n}\sum_{j=1}^{n}B_{ij}(0)\frac{N_j\delta}{\rho q_{j,\text{sat}}} = \sum_{i=1}^{n}\frac{N_i\delta}{\rho q_{i,\text{sat}}\mathcal{D}_i(0)} \tag{29}$$

Let us define a dimensionless total flux ϕ_{t} as

$$\phi_{\text{t}} \equiv \sum_{i=1}^{n}\frac{N_i\delta}{\rho q_{i,\text{sat}}\mathcal{D}_i(0)} \tag{30}$$

We note that the off-diagonal elements $B_{ij}(0)$ $(i \neq j)$ do not contribute to ϕ_{t}. As a consequence ϕ_{t} is independent of the loading and, therefore, η-invariant. Consequently, the linear differential equation (28) can be solved for the boundary conditions (19) and (20) by separation of variables to give the vacancy profile within the membrane

$$\left(\frac{(1/\theta_{\text{V}\eta}) - (1/\theta_{\text{V}0})}{(1/\theta_{\text{V}\delta}) - (1/\theta_{\text{V}0})}\right) = \frac{\exp(-\phi_{\text{t}}\eta) - 1}{\exp(-\phi_{\text{t}}) - 1} \tag{31}$$

where the term ϕ_{t} can be evaluated explicitly from

$$\phi_{\text{t}} \equiv \sum_{i=1}^{n}\frac{N_i\delta}{\rho q_{i,\text{sat}}\mathcal{D}_i(0)} = \ln\left(\frac{\theta_{\text{V}\delta}}{\theta_{\text{V}0}}\right) \tag{32}$$

It remains to solve Eq. (27) to obtain the π-profiles within the membrane. In order to do this we note that

$$\phi_i \equiv \sum_{j=1}^{n}B_{ij}(0)\frac{N_j\delta}{\rho q_{j,\text{sat}}} \tag{33}$$

are η-invariant for the special case of facile exchange, i.e. $\mathcal{D}_{ij} \to \infty$. For finite $\mathcal{D}_{ij}$, the assumption that ϕ_i are η-invariant is an excellent *approximation*, as we shall demonstrate later in the illustrative examples. Assuming ϕ_i to be η-invariant we can solve Eq. (27), after substituting Eq. (31), to obtain the component π-profiles

$$(\pi_{i\eta} - \pi_{i0}) = \frac{\exp(-\phi_{\text{t}}\eta) - 1}{\exp(-\phi_{\text{t}}) - 1}(\pi_{i\delta} - \pi_{i0}), \qquad i = 1, 2, \ldots, n \tag{34}$$

Table 1
Input parameters used in the illustrative Examples A and B. The density of the zeolite ρ is taken to be 1800 kg/m^3

Example	T (K)	Component	b_i (Pa^{-1})	$q_{i,\mathrm{sat}}$ (mol kg^{-1})	$Đ_i(0)/\delta$ (m/s)
A	303	C1	2.2×10^{-6}	2.24	2.6×10^{-5}
		C2	5.67×10^{-5}	1.85	3.75×10^{-6}
		C3	6.5×10^{-4}	1.58	8.5×10^{-6}
		n-C4	1.49×10^{-2}	1.61	2.5×10^{-7}
B	473	2-MP	1.27×10^{-4}	0.694	5×10^{-10}
		2,2-DMB	2.71×10^{-6}	0.694	6.25×10^{-12}

The corresponding loading profiles are obtained from

$$\theta_{i\eta} = \theta_{\mathrm{V}\eta}\pi_{i\eta}, \qquad q_{i,\eta} = \theta_{i\eta}q_{i,\mathrm{sat}}, \quad i = 1, 2, \ldots, n \tag{35}$$

Differentiating Eq. (34) and evaluating at the upstream face, we obtain after substituting into Eq. (26)

$$(N) = \frac{\rho}{\delta}\theta_{\mathrm{V}0}\frac{-\phi_{\mathrm{t}}}{\exp(-\phi_{\mathrm{t}}) - 1}[q_{\mathrm{sat}}][B_0(0)]^{-1}(\pi_0 - \pi_\delta) \tag{36}$$

where the subscripts 0 and δ emphasise the fact that the relevant parameters are evaluated at the upstream and downstream conditions, respectively. Substituting the expression (32) for ϕ_{t} we get after re-arrangement

$$(N) = \frac{\rho}{\delta}\frac{\ln(\theta_{\mathrm{V}\delta}/\theta_{\mathrm{V}0})}{(1/\theta_{\mathrm{V}0}) - (1/\theta_{\mathrm{V}\delta})}[q_{\mathrm{sat}}][B_0(0)]^{-1}(\pi_0 - \pi_\delta) \tag{37}$$

which allows explicit evaluation of the fluxes for the weak confinement scenario.

To illustrate the applicability of our analytic solution developed above let us consider permeation of a mixture of light alkanes, methane (C1), ethane (C2), propane (C3) and *n*-butane (*n*-C4) across an MFI membrane operating at 303 K. The Langmuir parameters and diffusivities of the components are specified in Table 1 (Example A). The downstream partial pressures of all components are fixed at 0.1 Pa. The partial pressures of C1, C2 and C3 in the upstream compartment are maintained at 85, 9, and 4 kPa, respectively. The partial pressure of *n*-C4 in the upstream compartment is varied in the range 1–2000 Pa. The numerical solution of the set of equations, for finite and infinite exchange coefficients $Đ_{ij}$, is presented as open symbols in Fig. 3; the details of the numerical procedure are available in earlier publications [3,10] and are on our web site: http://www.ct-cr4.chem.uva.nl/zeolites/. Calculations of the fluxes using Eq. (37), for finite and infinite exchange coefficients $Đ_{ij}$, are shown as continuous lines. For infinite – D_{ij}, the analytic solution given by Eq. (37) is *exact*, and there is precise correspondence between analytic and numerical solutions as is to be expected. For finite $Đ_{ij}$, the analytic solution given by Eq. (37) is *also* seen to be in excellent agreement with the numerical solution for all four components; this agreement points to the goodness of the assumption that ϕ_i is η-invariant in deriving the component loading profiles, Eq. (34). The results presented in Fig. 3 show that the fluxes of C1–C3 are all suppressed when the upstream partial pressure of *n*-C4 is increased; this is because *n*-C4 has much stronger adsorption strength and "hinders" the other species. We also note that finite interchange $Đ_{ij}$ tends to lead to significant lowering of the fluxes of C1 and C2. However, the flux of *n*-C4 is enhanced due to finite interchange $Đ_{ij}$. The experimental work of van de Graaf [13] has emphasised the importance of accounting for finite interchange $Đ_{ij}$ during permeation of light alkanes across an MFI membrane.

In order to appreciate the reasons behind the excellent agreement between numerical and analytic solutions, let us examine the component loading profiles for the case where the partial pressures in the upstream compartment are at 85, 9, 4 and 2 kPa, respectively, for the four components; see Fig. 4. The open symbols represent the profiles obtained from the precise numerical solution. The continuous lines represent the analytic solution given by Eq. (34). We note that even though the analytic solution deviates from the precise numerical solution as we proceed downstream in the membrane layer, the gradients of the loading at the upstream face are virtually the same. Therefore, evaluating the fluxes by using the loading gradients at the upstream face, rather than at the downstream face, yields accurate results for the fluxes following Eq. (37).

2.2. Analytic solution for strong confinement

For strong confinement we need to introduce the loading dependencies (4), (8) and (18) and the flux expression is

$$(N) = -\rho\theta_{\mathrm{V}}[q_{\mathrm{sat}}][B(0)]^{-1}[\Gamma]\frac{\partial(\theta)}{\partial z} \tag{38}$$

with the summation

$$\sum_{i=1}^{n}\sum_{j=1}^{n}B_{ij}\frac{N_j\delta}{\rho q_{j,\mathrm{sat}}} = \frac{1}{\theta_{\mathrm{V}}}\sum_{i=1}^{n}\sum_{j=1}^{n}B_{ij}(0)\frac{N_j\delta}{\rho q_{j,\mathrm{sat}}} = \frac{1}{\theta_{\mathrm{V}}}\sum_{i=1}^{n}\frac{N_i\delta}{\rho q_{i,\mathrm{sat}}Đ_i(0)} = \frac{\phi_{\mathrm{t}}}{\theta_{\mathrm{V}}} \tag{39}$$

where the η-invariant ϕ_{t} is defined by the same expression (30) as before. Substituting Eq. (39) into Eq. (28) we obtain the differential equation describing the vacancy profile

$$\frac{\partial(1/\theta_{\mathrm{V}})}{\partial\eta} = -\left(\frac{1}{\theta_{\mathrm{V}}}\right)^2\phi_{\mathrm{t}}, \qquad \frac{\partial\theta_{\mathrm{V}}}{\partial\eta} = \phi_{\mathrm{t}} \tag{40}$$

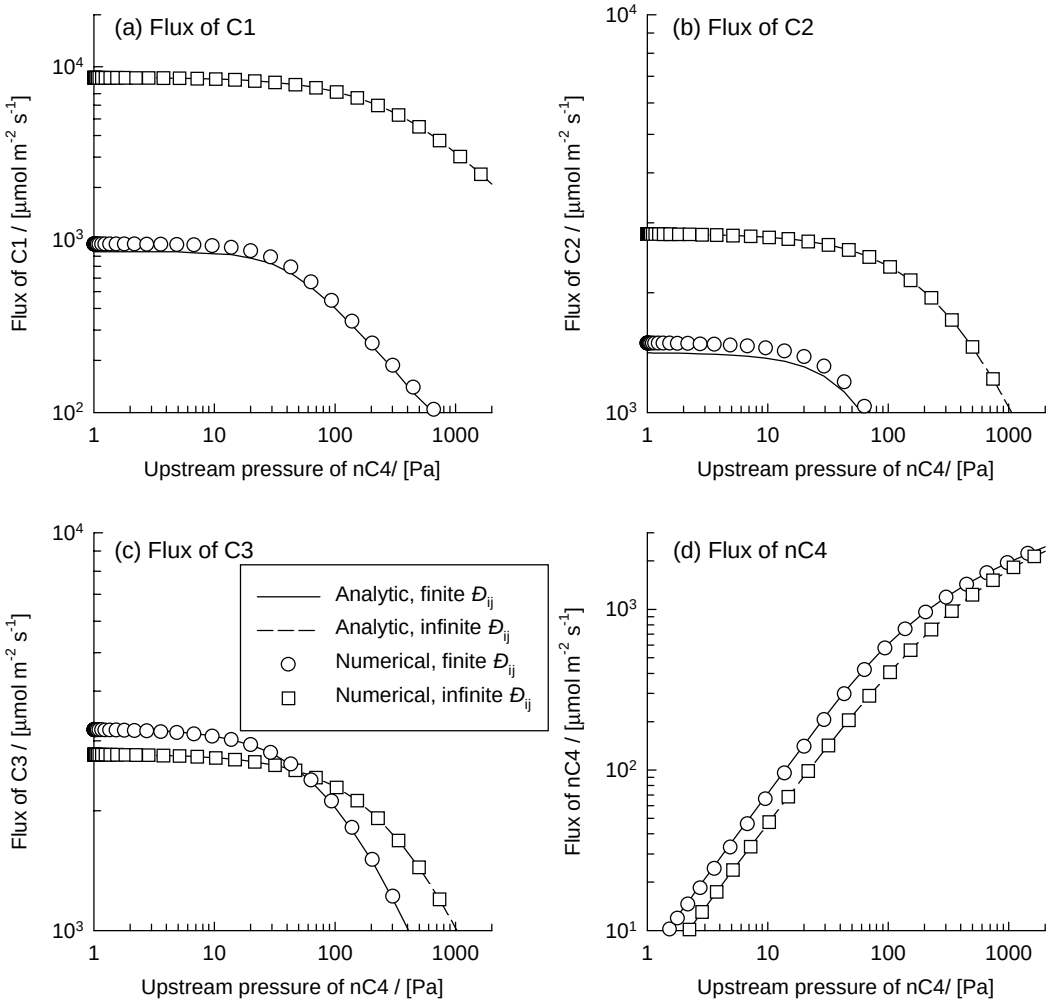

Fig. 3. Permeation fluxes for: (a) C1, (b) C2, (c) C3 and (d) *n*-C4 as a function of varying upstream partial pressure of *n*-C4. The upstream partial pressures of C1, C2, and C3 are 85, 9, and 4 kPa, respectively. Open symbols represent precise numerical solutions using the techniques described in our web site: http://www.ct-cr4.chem.uva.nl/zeolites/. The continuous lines represent calculations following Eq. (37). The weak confinement scenario prevails.

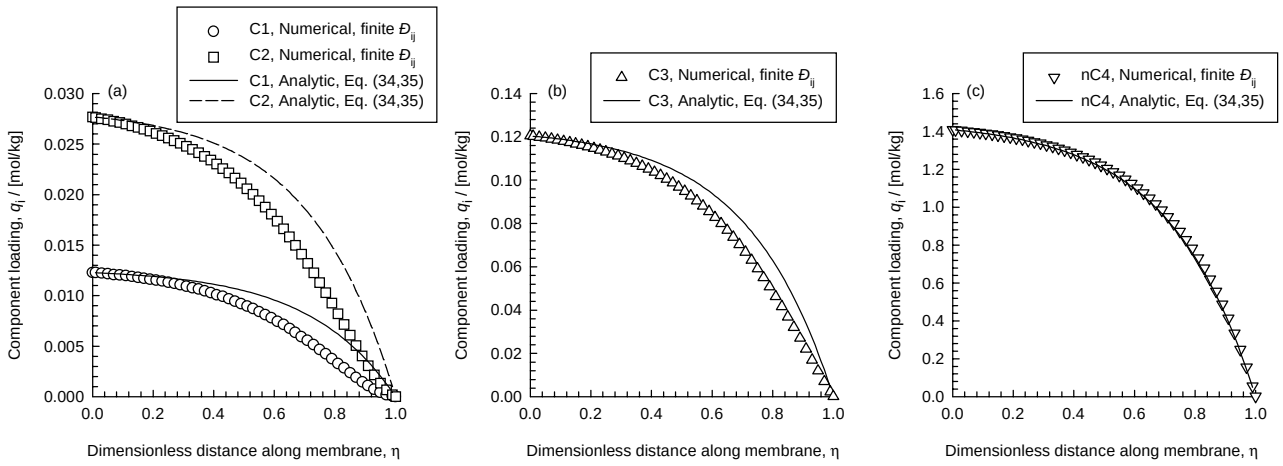

Fig. 4. Component loading profiles for: (a) C1 and C2, (b) C3 and (d) *n*-C4. The upstream partial pressures of C1, C2, C3 and *n*-C4 are 85, 9, 4 and 2 kPa, respectively. Open symbols represent precise numerical solutions using the techniques described in our web site: http://www.ct-cr4.chem.uva.nl/zeolites/. The continuous lines represent calculations following Eq. (34). The weak confinement scenario prevails.

which is a linear differential equation that can be solved for the boundary conditions (19) and (20) by separation of variables to give the profile

$$\left(\frac{\theta_{V\eta} - \theta_{V0}}{\theta_{V\delta} - \theta_{V0}}\right) = \eta \tag{41}$$

where the term ϕ_t can be evaluated explicitly from

$$\phi_t = \theta_{V\delta} - \theta_{V0} \tag{42}$$

With the *assumption* of η-invariant ϕ_i, defined by Eq. (33), the component loading profiles are linear:

$$\theta_{i\eta} = \theta_{i0} + \eta(\theta_{i\delta} - \theta_{i0}),$$
$$q_{i,\eta} = \theta_{i\eta} q_{i,sat}, \quad i = 1, 2, \ldots, n \tag{43}$$

the above equation represents the exact solution for facile exchange, i.e. $Đ_{ij} \to \infty$.

Differentiating Eq. (43) and evaluating at the upstream face, we obtain after substituting into Eq. (26)

$$(N) = \frac{\rho}{\delta}\theta_{V0}\theta_{V\delta}[q_{sat}][B_0(0)]^{-1}(\pi_0 - \pi_\delta) \tag{44}$$

where the subscripts 0 and δ emphasise the fact that the relevant parameters are evaluated at the upstream and downstream conditions, respectively.

To illustrate the applicability of Eq. (44) let us consider permeation of a mixture of 2-methylpentane (2-MP) and 2,2-dimethylbutane (2,2-DMB) across an MFI membrane operating at 473 K. The Langmuir parameters and diffusivities of the components are specified in Table 1 (Example B). The downstream partial pressures of both components are fixed at 0.1 Pa. Two cases are examined. In the first case (see Fig. 5(a) and (b)), the upstream partial pressure of 2,2-DMB is maintained at 50 kPa and the partial pressure of 2-MP is varied in the range 0.1–50 kPa. In the second case (see Fig. 5(c) and (d)), the upstream partial pressure of 2-MP is maintained at 50 kPa and the partial pressure of 2,2-DMB is varied in the range 0.1–50 kPa. The numerical solution of the set of equations, for finite and infinite exchange coefficients $Đ_{ij}$, is presented as open symbols in Fig. 5; the details of the numerical procedure are available in earlier publications [3,10]. The calculation of the fluxes using Eq. (44) for finite and infinite exchange coefficients $Đ_{ij}$ are shown as continuous lines. For infinite $Đ_{ij}$, the analytic solution given by

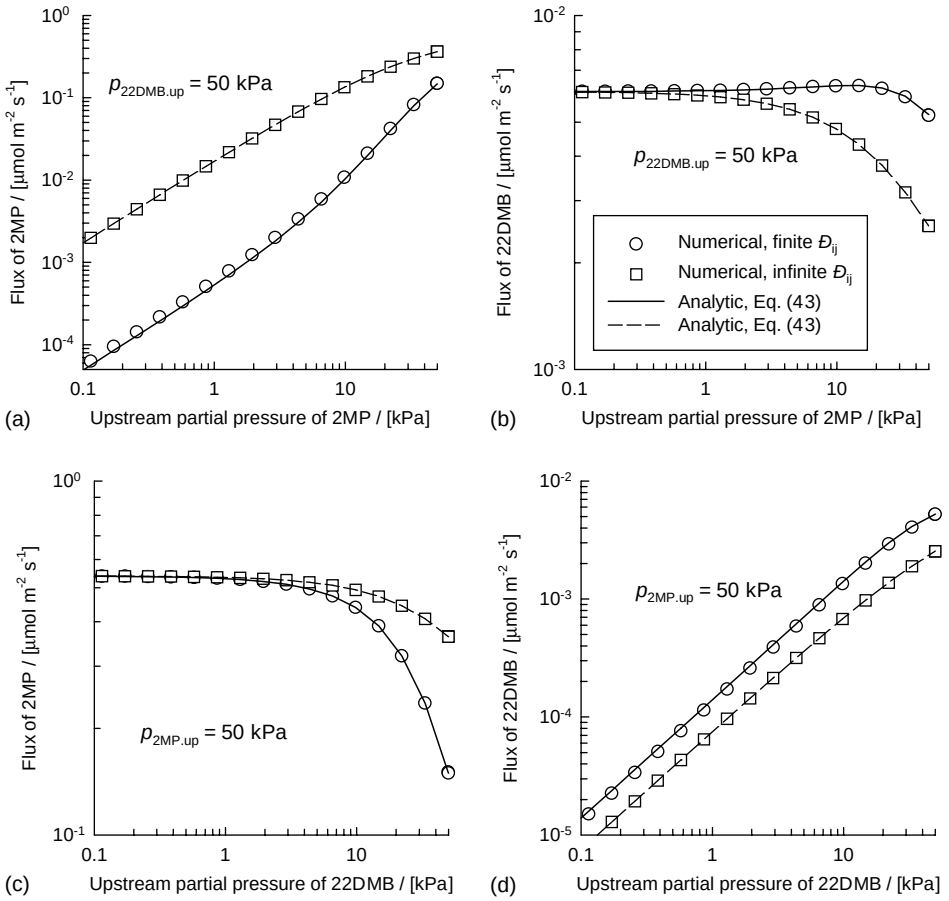

Fig. 5. Permeation fluxes for 2-MP and 2,2-DMB. In (a) and (b) the upstream partial pressure of 2,2-DMB is maintained at 50 kPa and the partial pressure of 2-MP is varied in the range 0.1–50 kPa. In (c) and (d) the upstream partial pressure of 2-MP is maintained at 50 kPa and the partial pressure of 2,2-DMB is varied in the range 0.1–50 kPa. Open symbols represent precise numerical solutions using the techniques described in our web site: http://www.ct-cr4.chem.uva.nl/zeolites/. The continuous lines represent calculations following Eq. (44). The strong confinement scenario prevails.

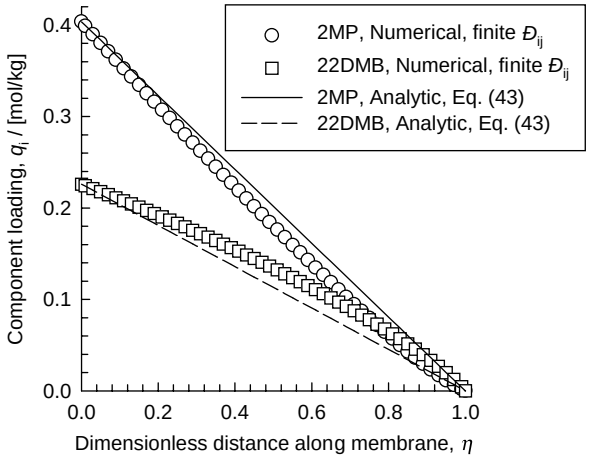

Fig. 6. Component loading profiles for 2-MP and 2,2-DMB. The upstream partial pressures of 2-MP and 2,2-DMB are both 50 kPa. Open symbols represent precise numerical solutions using the techniques described in our web site: http://www.ct-cr4.chem.uva.nl/zeolites/. The continuous lines represent calculations following Eqs. (43) and (44). The strong confinement scenario prevails.

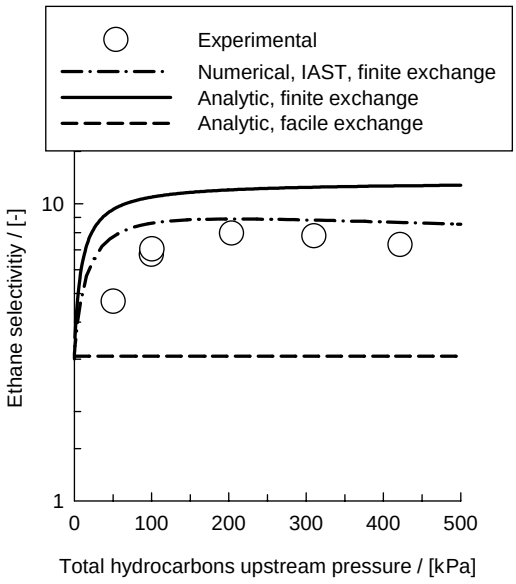

Fig. 7. Ethane selectivity for permeation of 50–50 mixtures of methane–ethane across an MFI membrane at 303 K. The experimental data in Fig. 6(b) of Ref. [13] are compared with the analytic model for finite exchange (solid lines) and facile exchange (dashed lines). We assume weak confinement scenario. The dot-dashed lines are the calculations of the numerical solution in which the mixture loadings are calculated using the IAST. The parameter values are the same as used in Example A and listed in Table 1.

Eq. (44), is *exact*, and there is precise correspondence between analytic and numerical solutions, as is to be expected. For finite $Đ_{ij}$, the analytic solution given by Eq. (44), is *also* seem to be in excellent agreement with the numerical solution; this agreement points to the goodness of the assumption that ϕ_i is η-invariant in deriving the component loading profiles, Eq. (43).

In order to appreciate the reasons behind this good agreement, let us examine the component loading profiles for the case where the partial pressures in the upstream compartment are 50 kPa for both components; see Fig. 6. The open symbols represent the profiles obtained from the precise numerical solution. The continuous lines represent the analytic solution given by Eq. (43). We note that even though the analytic solution deviates from the precise numerical solution as we proceed downstream in the membrane layer, the gradients of the component loadings at the upstream face are the same. Therefore, evaluating the fluxes by using the loading gradients at the upstream face, rather than at the downstream face, yields accurate results for the fluxes following Eq. (44).

3. Comparison with experiment

In order to stress the practical utility, and limitations, of the analytic model developed above we consider the experimental data of van de Graaf et al. [13] for the ethane selectivity for permeation of 50–50 mixtures of methane–ethane across an MFI membrane at 303 K. For varying total hydrocarbons pressure in the upstream compartment (see data in Fig. 6(b) of Ref. [13]) the experimental values of the ethane selectivity, defined as the ratio of the permeation fluxes of ethane with respect to methane, are shown as open symbols in Fig. 7. Also shown in Fig. 7 are the analytic model calculations for the ethane selectivity using Eq. (37) for weak confinement, for finite exchange (shown as solid lines) and facile exchange (shown as dashed lines). The data inputs are the same as used for Example A in Table 1. The facile exchange model severely underestimates the ethane selectivity, and predicts ethane selectivity values of the order of 3. On the other hand, the finite exchange model takes proper account of the slowing down of the more mobile methane, leading to significantly higher selectivities of the order of 10, much closer to the experimental values of around 8.

It is important to stress here that the analytic model developed in this paper is restricted to the use of the multicomponent Langmuir equations (11) for calculating mixture loadings. For mixtures with different saturation capacities, the multicomponent Langmuir model is not thermodynamically consistent and for more accurate calculations we should use the ideal adsorbed solution theory (IAST) of Myers and Prausnitz [33]; this point has been stressed by Kapteijn et al. [9]. Calculations of the ethane selectivity incorporating the IAST, following the numerical solutions described on our web site: http://www.ct-cr4.chem.uva.nl/zeolites/ are shown in Fig. 7 as dotted lines. We note that much better agreement with the experimental data is obtained with the IAST.

4. Conclusions

Analytic solutions have been derived for the explicit calculation of the permeation fluxes across a zeolite membrane.

Diffusion within the membrane layer is described by the Maxwell–Stefan equations. The loading dependence of the M–S diffusivities of the pure components, $Đ_i$, are assumed to follow either the weak or strong confinement scenarios, described by Eqs. (3) and (4), respectively. The derived analytic solutions are *exact* for the case of infinite exchange – D_{ij}. The illustrative examples show that the calculation of the fluxes using Eq. (37) for weak confinement, or Eq. (44) for strong confinement, are in excellent agreement with precise numerical calculations for both finite and infinite $Đ_{ij}$.

The developed analytic expressions can be easily incorporated into design procedures for membrane separation devices and membrane reactors. For mixtures with widely different saturation capacities, calculations of our analytic Langmuir model may be less accurate than the more rigorous IAST, for which numerical solutions will be required.

Acknowledgements

RK and RB acknowledge a grant Programmasubsidie from The Netherlands Foundation for Fundamental Research (CW-NWO) for development of novel concepts in reactive separations.

References

[1] J. Caro, M. Noack, P. Kolsch, R. Schafer, Zeolite membranes—state of their development and perspective, Micropor. Mesopor. Mater. 38 (2000) 3–24.
[2] J. Coronas, J. Santamaria, Separations using zeolite membranes, Sep. Purif. Meth. 28 (1999) 127–177.
[3] R. Krishna, D. Paschek, Separation of hydrocarbon mixtures using zeolite membranes: a modelling approach combining molecular simulations with the Maxwell–Stefan theory, Sep. Purif. Technol. 21 (2000) 111–136.
[4] M.P. Bernal, J. Coronas, M. Menendez, J. Santamaria, Coupling of reaction and separation at the microscopic level: esterification processes in a H-ZSM-5 membrane reactor, Chem. Eng. Sci. 57 (2002) 1557–1562.
[5] R. Krishna, Diffusion of binary mixtures across zeolite membranes: entropy effects on permeation selectivity, Int. Commun. Heat Mass Transfer 28 (2001) 337–346.
[6] R. Krishna, Predicting transport diffusivities of binary mixtures in zeolites, Chem. Phys. Lett. 355 (2002) 483–489.
[7] R. Krishna, D. Paschek, Self-diffusivities in multicomponent mixtures in zeolites, Phys. Chem. Chem. Phys. 4 (2002) 1891–1898.
[8] R. Krishna, J.A. Wesselingh, The Maxwell–Stefan approach to mass transfer, Chem. Eng. Sci. 52 (1997) 861–911.
[9] F. Kapteijn, J.A. Moulijn, R. Krishna, The generalized Maxwell–Stefan model for diffusion in zeolites: sorbate molecules with different saturation loadings, Chem. Eng. Sci. 55 (2000) 2923–2930.
[10] R. Krishna, L.J.P. Van den Broeke, The Maxwell–Stefan description of mass-transport across zeolite membranes, Chem. Eng. J. 57 (1995) 155–162.
[11] R. Krishna, R. Baur, Modelling issues in zeolite based separation processes, Sep. Purif. Technol., in press.
[12] B. Smit, R. Krishna, Molecular simulations in zeolitic process design, Chem. Eng. Sci. 58 (2003) 557–568.
[13] J.M. van de Graaf, F. Kapteijn, J.A. Moulijn, Modeling permeation of binary mixtures through zeolite membranes, AIChE J. 45 (1999) 497–511.
[14] R. Krishna, D. Paschek, Permeation of hexane isomers across ZSM-5 zeolite membranes, Ind. Eng. Chem. Res. 39 (2000) 2618–2622.
[15] P. Ciavarella, H. Moueddeb, S. Miachon, K. Fiaty, J.A. Dalmon, Experimental study and numerical simulation of hydrogen/isobutane permeation and separation using MFI-zeolite membrane reactor, Catal. Today 56 (2000) 253–264.
[16] B. Millot, A. Methivier, H. Jobic, H. Moueddeb, J.A. Dalmon, Permeation of linear and branched alkanes in ZSM-5 supported membranes, Micropor. Mesopor. Mater. 38 (2000) 85–95.
[17] T.Q. Gardner, J.L. Falconer, R.D. Noble, M. Zieverink, Analysis of transient permeation fluxes into and out of membranes for adsorption measurements, Chem. Eng. Sci. 58 (2003) 2103–2112.
[18] P.J.A.M. Kerkhof, Partial analytical solutions for steady-state diffusion in zeolite membranes, AIChE J. 44 (1998) 1697–1700.
[19] D. Paschek, R. Krishna, Kinetic Monte Carlo simulations of transport diffusivities of binary mixtures in zeolites, Phys. Chem. Chem. Phys. 3 (2001) 3185–3191.
[20] R. Krishna, D. Paschek, Verification of the Maxwell–Stefan theory for diffusion of three-component mixtures in zeolites, Chem. Eng. J. 87 (2002) 1–9.
[21] F.J. Keil, R. Krishna, M.O. Coppens, Modeling of diffusion in zeolites, Rev. Chem. Eng. 16 (2000) 71–197.
[22] D.M. Ruthven, Principles of Adsorption and Adsorption Processes, Wiley, New York, 1984.
[23] J. Kärger, D.M. Ruthven, Diffusion in Zeolites and Other Microporous Solids, Wiley, New York, 1992.
[24] D.M. Ruthven, M.F.M. Post, Diffusion in zeolite molecular sieves, in: H. van Bekkum, E.M. Flanigan, P.A. Jacobs, J.C. Jansen (Eds.), Introduction to Zeolite Science and Practice, vol. 137, Elsevier, Amsterdam, 2001, Chapter 12, pp. 525–577.
[25] E.J. Maginn, A.T. Bell, D.N. Theodorou, Transport diffusivity of methane in silicalite from equilibrium and nonequilibrium simulations, J. Phys. Chem. 97 (1993) 4173–4181.
[26] A.I. Skoulidas, D.S. Sholl, Direct tests of the Darken approximation for molecular diffusion in zeolites using equilibrium molecular dynamics, J. Phys. Chem. B 105 (2001) 3151–3154.
[27] A.I. Skoulidas, D.S. Sholl, Transport diffusivities of CH_4, CF_4, He, Ne, Ar, Xe and SF_6 in silicalite from atomistic simulations, J. Phys. Chem. B 106 (2002) 5058–5067.
[28] D. Paschek, R. Krishna, Monte Carlo simulations of self- and transport-diffusivities of 2-methylhexane in silicalite, Phys. Chem. Chem. Phys. 2 (2000) 2389–2394.
[29] D. Paschek, R. Krishna, Inter-relation between self- and jump-diffusivities in zeolites, Chem. Phys. Lett. 333 (2001) 278–284.
[30] R. Krishna, D. Paschek, Verification of the Maxwell–Stefan theory for tracer diffusion in zeolites, Chem. Eng. J. 85 (2002) 7–15.
[31] J. Kärger, S. Vasenkov, S.M. Auerbach, Diffusion in zeolites, in: S.M. Auerbach, K.A. Carrado, P.K. Dutta (Eds.), Handbook of Zeolite Science and Technology, Marcel Dekker, New York, 2003, Chapter 10.
[32] D. Paschek, R. Krishna, Monte Carlo simulations of sorption and diffusion of isobutane in silicalite, Chem. Phys. Lett. 342 (2001) 148–154.
[33] A.L. Myers, J.M. Prausnitz, Thermodynamics of mixed gas adsorption, AIChE J. 11 (1965) 121–130.